Journal of Macromolecular Science, Part A
Publication details, including instructions for authors and subscription information:
http://www.informaworld.com/smpp/title~content=t713597274

Structure and Properties of Polyamide-6 & 6/66 Clay Nanocomposites

Sriram Venkataramani[a]; Jae Heung Lee[b]; Min Gyoo Park[a]; Sung Chul Kim[a]
[a] Center for Advanced Functional Polymers, Department of Chemical and Bimolecular Engineering, Korea Advanced Institute of Science and Technology, Yuseong-Gu, Daejeon, Korea [b] Advanced Materials Division, Korea Research Institute of Chemical Technology, Yuseong, Daejeon, Korea

To cite this Article Venkataramani, Sriram , Lee, Jae Heung , Park, Min Gyoo and Kim, Sung Chul(2009) 'Structure and Properties of Polyamide-6 & 6/66 Clay Nanocomposites', Journal of Macromolecular Science, Part A, 46: 1, 65 — 73
To link to this Article: DOI: 10.1080/10601320802515399
URL: http://dx.doi.org/10.1080/10601320802515399

Journal of Macromolecular Science®, Part A: Pure and Applied Chemistry (2009) **46**, 65–73

ISSN: 1060-1325 print / 1520-5738 online
DOI: 10.1080/10601320802515399

Taylor & Francis
Taylor & Francis Group

Structure and Properties of Polyamide-6 & 6/66 Clay Nanocomposites

SRIRAM VENKATARAMANI,[1#] JAE HEUNG LEE,[2] MIN GYOO PARK[1] and SUNG CHUL KIM[1,*]

[1] *Center for Advanced Functional Polymers, Department of Chemical and Bimolecular Engineering, Korea Advanced Institute of Science and Technology, 373-1, Guseong-Dong, Yuseong-Gu, Daejeon 305-701, Korea*
[2] *Advanced Materials Division, Korea Research Institute of Chemical Technology, P.O.Box 107, Yuseong, Daejeon 305-600, Korea*

Received June 2008, Accepted July 2008

The structural, morphological and thermal properties of polyamide-6 and polyamide-6/66 clay nanocomposites have been studied using X-ray diffraction (XRD), transmission electron microscopy (TEM), scanning electron microscopy (SEM), differential scanning calorimetry (DSC), thermogravimetric analysis (TGA) and static and dynamic mechanical analysis. The wide-angle X-ray diffraction (WAXRD) and TEM results show the effects of clay loading in the polymer matrix. The polyamide-6 series show coexistence of intercalated and exfoliated structures and the polyamide-6/66 series show a complete exfoliated structure. Both series show the presence of a structural crystal phase transition. The dispersibility of organoclay in polyamide polymer and copolymer matrix is in agreement with the TEM image results. With an increase in clay content, there is a transformation from α to γ form of the polyamide-6 crystals. SEM observation indicates that the silicate particles are homogeneously dispersed in the polymer matrix without significant agglomeration even with an increase in clay loading. Thermogravimetric analysis reveals that the thermal stability increases with an increase in the clay content. DSC results show that as the clay content increases, the crystallization temperature increases, due to a strong heterophase nucleation effect. Static mechanical analysis show that the tensile strength, tensile modulus, heat distortion temperature and flexural strength increase with increase in clay loading for both the polyamide-6 and polyamide-6/66 series. On the other hand, elongation and impact decrease with an increase in clay loading in both the polyamide-6 and 6/66 series.

Keywords: Polyamide 6, clay nanocomposites, morphology, crystallization temperature, thermal stability

1 Introduction

Polymer nanocomposites have been an area of intense industrial and academic research interest for the past 20 years. These nanocomposites represent a radical alternative to conventional filled polymers, or polymer blends. They offer tremendous improvement in a wide range of physical and engineering properties for polymers with low filler loading. Growing research interests are focused on hybrid materials consisting of polymers containing nanoscale inorganic fillers (1). Polymer composites have been widely used in areas of electronics, transportation, construction and consumer products. They offer an unusual combination of stiffness and toughness that is difficult to attain for single polymer materials. Polyamide 6/clay nanocomposites (PA6CN) based on montmorillonite are interesting materials since they exhibit unexpected hybrid properties synergistically derived from two components. The first successful example of a nylon-clay hybrid (NCH) was found and developed at Toyota Central Research and Development Laboratory (2–4) 17 years ago. From then on, many investigations have been carried out on the preparation, mechanical properties (5–7), effect of addition of clay on the crystalline structures, morphology (8–13), thermal degradation (14), rheology (15–16) and flame retardation (17). Thus, one of the exciting and promising developments in material science today is the design and synthesis of organic-inorganic nanocomposites that possess enhanced and novel properties which are unattainable with the organic and inorganic material alone (18–21).

One of the most remarkable features of Polyamide 6 (PA6) is that this semicrystalline polymer exhibits polymorphism depending on the thermal history, processing conditions, mechanical stress, crystallization conditions, etc. Studies on the crystal structure of PA6 in nanocomposites were first carried out by Kojima et al. (22). Usually the two complementary characterization techniques used for polymer/clay nanocomposites are X-ray diffraction (XRD) and

*Address correspondence to: Sung Chul Kim, Center for Advanced Functional Polymers, Department of Chemical and Bimolecular Engineering, Korea Advanced Institute of Science and Technology, 373-1, Guseong-Dong, Yuseong-Gu, Daejeon 305-701, Korea. E-mail: kimsc@kaist.ac.kr
#Present address: Aortech Biomaterials Pty Ltd, Melbourne, Australia

Table 1. Materials used in this study

Material [designation used]	$M_w^{*1}/10^4$	M_w/M_n^{*1}	*Clay content (%)*	*Ash**2 *(wt %)*
Polyamide 6 (Y0)	3.85	1.71	0	-
Polyamide 6 (Y2)	3.95	1.74	2	1.74
Polyamide 6 (Y4)	3.56	1.80	4	4.37
Polyamide 6 (Y5)	3.51	1.78	5	5.29
Polyamide 6(UH0)	5.74	1.80	0	-
Polyamide 6 (UH2)	5.77	1.90	2	1.71
Polyamide 6/66(UCO)*3	6.68	1.87	0	-
Polyamide 6/66 (UC2)*3	5.56	1.92	2	1.56

*1 Measured by GPC calibrated with PMMA standards.
*2 10g pellets were burned to ashes.
*3 6/66 = 80/20 copolymer.

transmission electron microscopy (TEM) (23). Several researchers have reported intensive research efforts recently devoted to the effect of clay on the crystallization behavior of PA6 matrix (24–26). In this paper, we study the nanostructure and morphology of polyamide-6 and polyamide-6/66 (PA6/66) nanocomposites by using XRD, TEM in order to understand the effect of clay loading on their structure and properties.

2 Experimental

2.1 Materials and Characterization

Polyamide 6 (Y0, UH0) and copolymer 6/66 (UC0) and their layered-silicate nanocomposites with clay of 2% (Y2, UH2, UC2), 4% (Y4) and 5% (Y5), respectively were originally supplied by UBE and UNITIKA Ltd. (Japan) in the form of pellets (Table 1). The as-received samples were dried under vacuum at 80°C for 48 h prior to all the characterizations. For XRD measurements, the dried pellets were subjected to compression molding in the form of small circular discs at 20°C above the melting temperature of PA6 (220°C). For XRD and DMTA measurements, the dried pellets were subjected to compression molding in the form of small circular discs for XRD measurements and rectangular strips ($10 \times 30 \times 1.8$ mm) of each material for DMTA measurements at 20°C above the melting temperature of PA6. For static mechanical study, the dried pellets were subjected to injection molding to dumb-bell shaped specimens (five specimens each) of the dimensions $3.15 \times 12.85^* \times 63^*$ mm (* - width and length of a narrow section of the dumb-bell specimen) for testing. Thermal analysis was performed using a TA instruments DSC Q_{100} with refrigerated cooling accessory. The mass of each sample was 7–10 mg. The samples were subjected to heating and cooling cycles in the temperature range from −80°C to +300°C at a rate of $10°C.min^{-1}$ under an ultrapure nitrogen atmosphere. Thermogravimetric analysis was

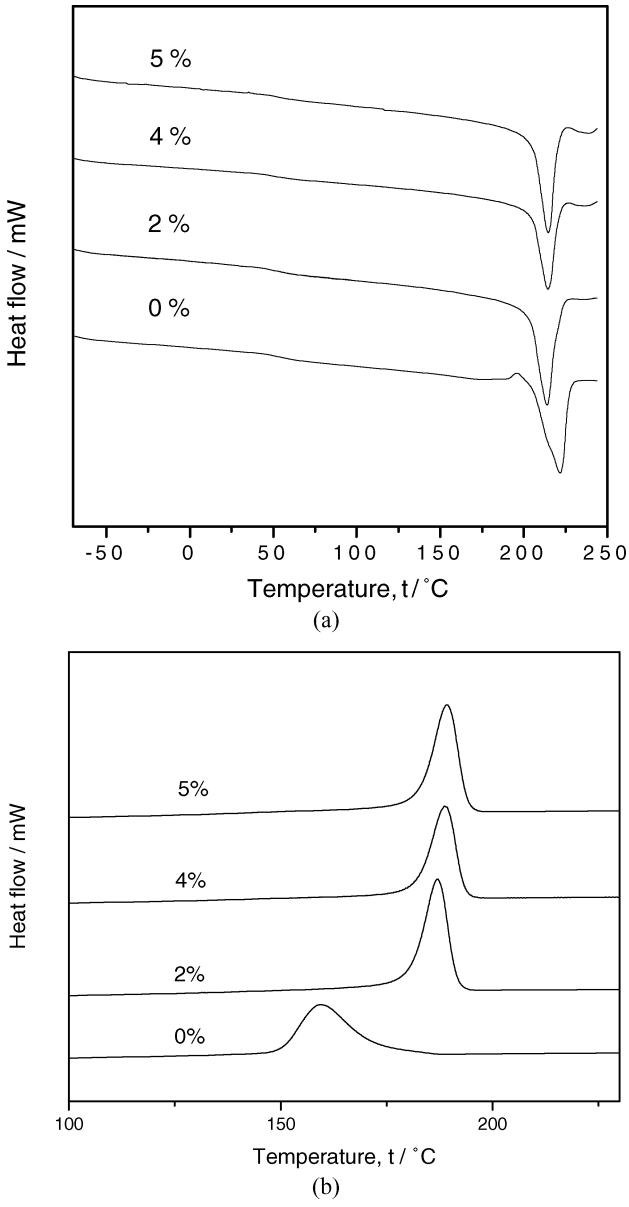

Fig. 1. DSC for PA6 (Y series) (a) Heating curves, (b) cooling curves.

Table 2. Thermal Properties of PA6, 6/66/Clay Nanocomposites

Polymer Code	$T_g/°C$	$T_m/°C$	$T_c/°C$	$\Delta_{fus}H/J.g^{-1}$	$T_{95}^*(°C)$ *in* N_2
Y0	53.9	221.8	159.3	58.4	432
Y2	53.6	213.8	187.6	51.9	433
Y4	53.9	214.8	189.0	46.1	434
Y5	53.9	214.6	189.7	40.9	437
UH0	52.2	220.9	157.6	51.6	416
UH2	53.9	214.4	180.2	50.8	416.4
UC0	51.1	193.5	118.7	32.8	419.5
UC2	50	191.7	150.7	30.7	421.3

*T_{95}: temperature with 95% weight retention

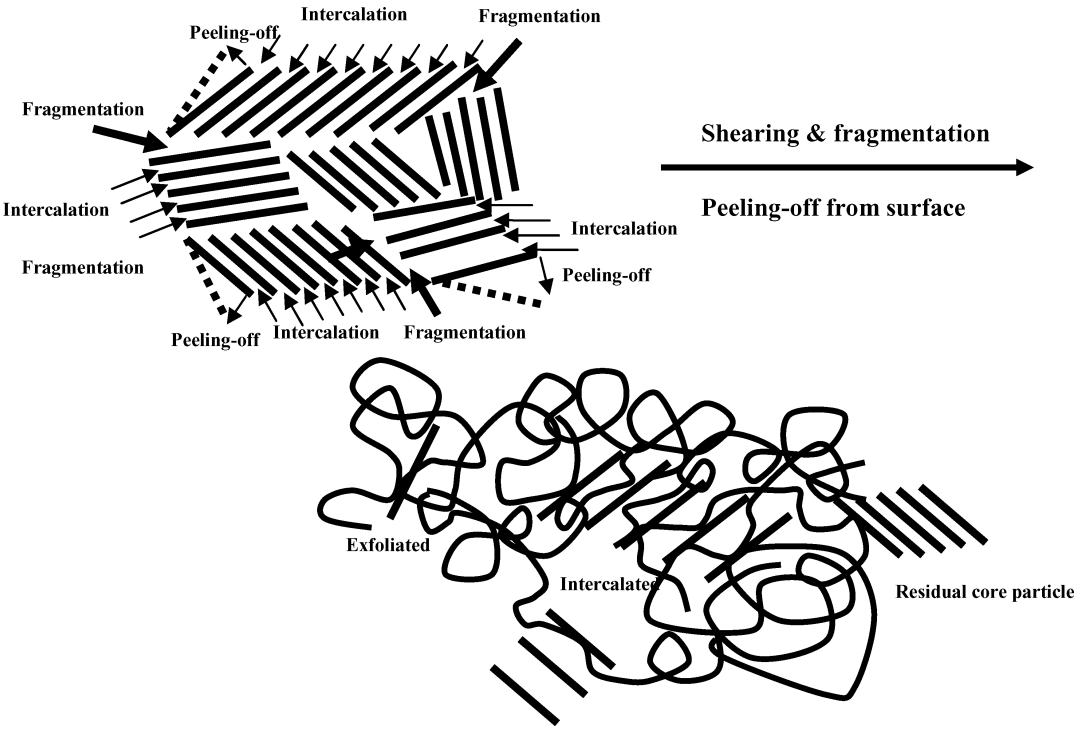

Fig. 2. Schematic picture showing the peeling-off process.

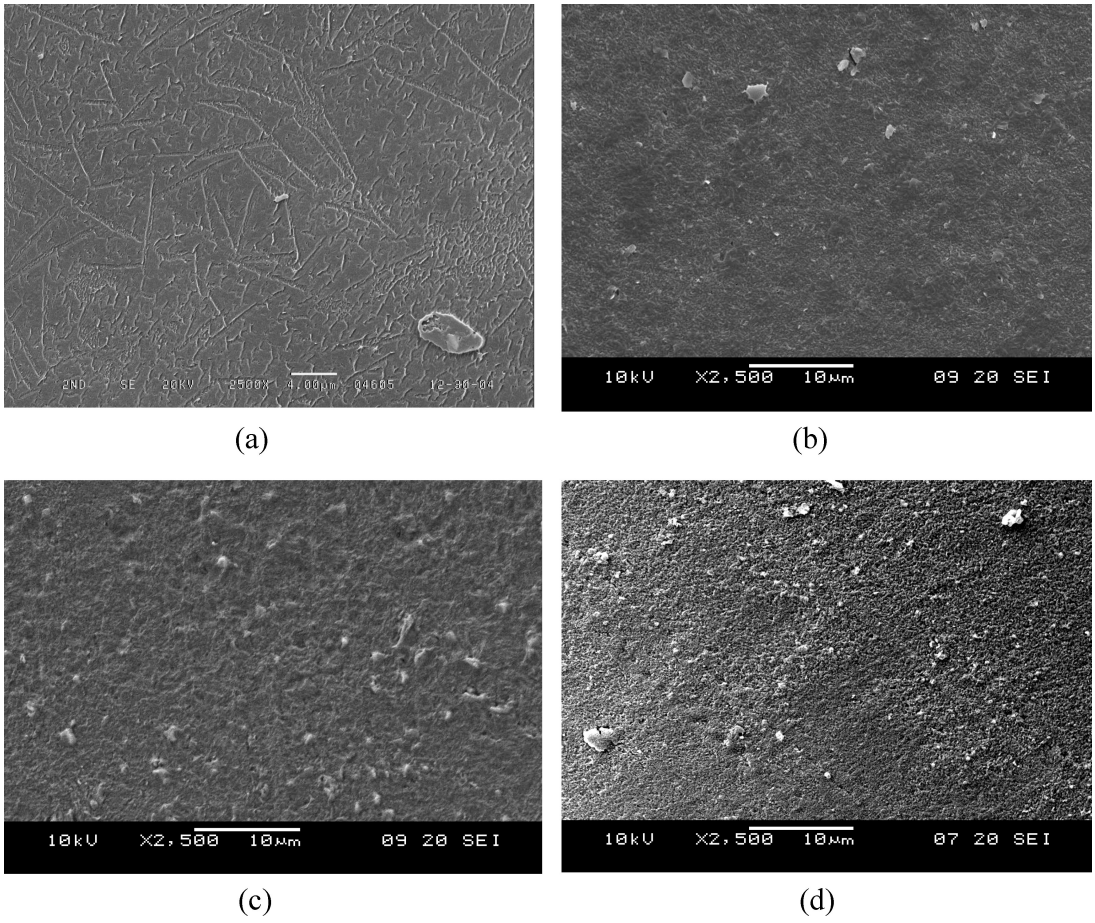

Fig. 3. SEM micrographs of surface morphology for: (a) Y0, (b) Y2, (c) Y4, (d) Y5.

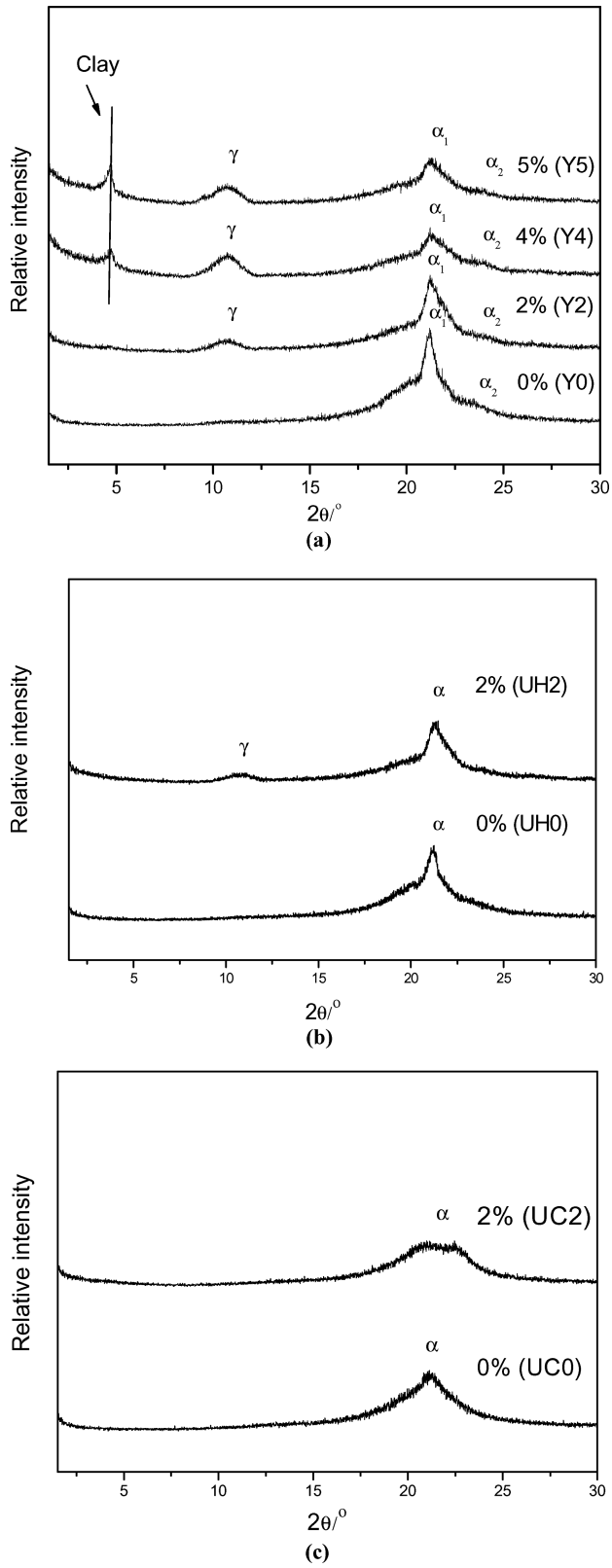

Fig. 4. WAXRD patterns for (a) PA6 (Y series), (b) PA6 (UH series) and (c) PA6/66 (UC series).

Table 3. TEM analysis results of PA6 samples

	Polymer Code		
Clay platelets	*Y2*	*Y4*	*Y5*
Particle population[a] / μm^{-2}	77	111	133
Average thickness/nm	2.95	4.07	4.08
Std Dev of thickness/nm	1.44	1.33	1.33

[a]The particle population is the average number of momtmorillonite particles per μm^2.

performed under nitrogen atmosphere and air by using a TA instruments TGA Q_{500} to measure the thermal stability of PA6 & PA6/66 and its nanocomposites. The measurement was carried out with a heating rate of 20 °C.min^{-1} in the temperature range from 50°C to 700°C. Wide-angle X-ray diffraction was conducted at ambient temperature on a Rigaku D/MAX-RC diffractometer with Cu K_α radiation to measure the *d*-spacing of silicate layers. Each sample was scanned from $2\theta = 1.2$ to 30° at a scan rate of 2° min^{-1}. SEM specimens were subjected to plasma etching by treating in a POLARON PT7160 plasma reactor. The surface of the samples was etched under vacuum 1 Pa in oxygen plasma (RF power 50 watt). The etched surface of the samples was then observed using a Jeol JSM-5610 SEM, after gold coating, to determine the dispersability of clay. TEM specimens were prepared by using a RMC MT-XL microtome with a cryogenic CR-XL system. The specimens were cut with a diamond knife at −100°C. TEM micrographs were obtained using a Philips CM20 transmission electron microscope. Static mechanical tests were carried out with an Instron model 4482 UTM according to ASTM D638 for measuring tensile strength (TS; crosshead speed at 50 mm.min^{-1}), elongation (ε), tensile modulus (TM) and elongation, ASTM D790 for measuring flexural strength (FS; crosshead speed at 10 mm.min^{-1}), flexural modulus (FM), ASTM D256 for impact measurement and ASTM D648 for heat distortion temperature (HDT) measurement at the heating rate of 2°C min^{-1}.

3 Results and Discussion

3.1 Thermal Studies

The thermal properties of polyamide-6 & 6/66 and its nancomposites were determined by thermogravimetric analysis (TGA) and differential scanning calorimetry (DSC). The TGA thermograms for the virgin samples and its nanocomposites were obtained in nitrogen atmospheres. It can be seen from Table 2 that the thermal stability of the virgin nylon (PA6, PA6/66) and its clay nanocomposite up to 5% loading did not show significant differences.

Representative DSC cooling and heating curves of polyamide-6 (Y series) are given in Figures 1a and 1b. The DSC measurements indicate that the presence of clay does

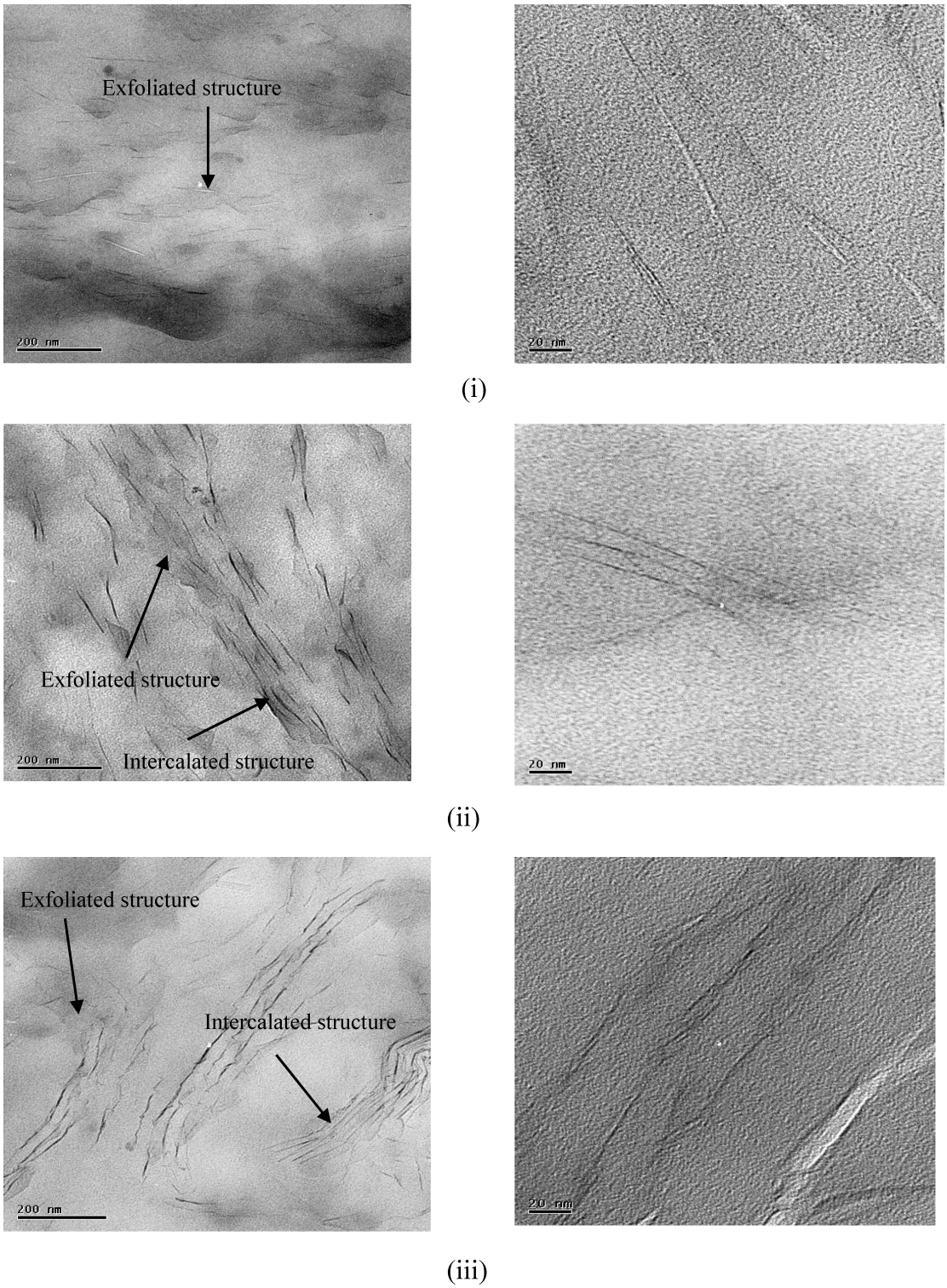

Fig. 5a. TEM images showing the nanostructures in polyamide nanocomposites for clay content of (i) Y2, (ii) Y4, (iii) Y5.

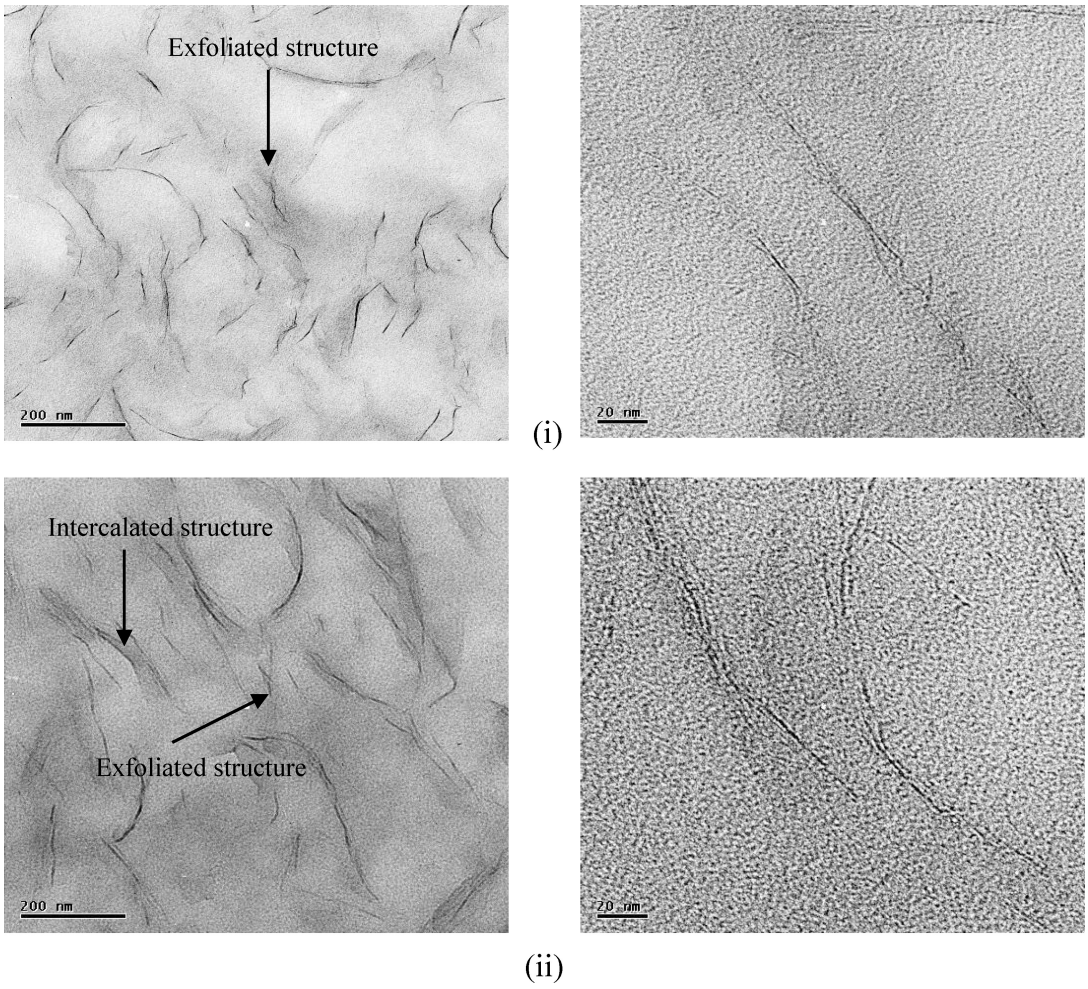

Fig. 5b. TEM image showing the nanostructures in polyamide nanocomposites for clay content of (i) UH2, (ii) UC2.

not have any significant influence on the T_g (glass transition temperature) of the PA6 matrix which occurs at approximately 53.9°C. The DSC melting peak (T_m) (Fig. 1a) of the nanocomposites occurs at a slightly lower temperature than that of PA6. This may be related to a slight reduction in crystallite size with the presence of clay in the nanocomposites (27, 28). The presence of clay in the nanocomposites causes an increase in the crystallization temperature (T_c) and narrows the width of crystalline peaks (Fig. 1b) relative to PA6. This is due to the strong heterophase nucleation effect. The heat of fusion (ΔH_{fus}) decreases with increase in clay content in the PA6 and PA6/66 series. Thus strongly suggests a good dispersion between the polymer and clay. Table 2 provides a summary of the results.

Table 4. Mechanical properties of PA6, 6/66/clay Nanocomposites

Code	*TS/MPa*	*TM/GPa*	*FS/MPa*	*FM/GPa*	*Relative elongation, ε/%*	*Impact/J m^{-1}*	*HDT(°C)*
Y0	82.1 ± 0.6	1.3 ± 0.04	108.1 ± 0.8	2.8 ± 0.04	73.3 ± 13.8	46.2 ± 4.2	176.4 ± 1.1
Y2	82.7 ± 0.8	1.5 ± 0.17	117.7 ± 0.4	3.5 ± 0.06	62.3 ± 4.6	41.7 ± 1.4	190.9 ± 1.5
Y4	92.7 ± 3.4	2.0 ± 0.09	134.1 ± 0.7	4.6 ± 0.05	5.4 ± 0.5	35.7 ± 0.6	197.0 ± 0.5
Y5	95.0 ± 4.0	2.2 ± 0.24	137.2 ± 1.4	4.9 ± 0.15	4.4 ± 0.4	34.4 ± 2.2	198.2 ± 0.1
UH0	64.8 ± 4.6	1.1 ± 0.11	74.6 ± 0.9	1.9 ± 0.02	269.7 ± 35.1	88.0 ± 10.7	169.7 ± 2.6
UH2	79.3 ± 5.7	1.6 ± 0.17	113.0 ± 0.5	3.1 ± 0.08	110.3 ± 21.9	55.6 ± 9.1	190.5 ± 0.3
UC0	53.6 ± 3.5	1.0 ± 0.07	43.5 ± 2.3	1.1 ± 0.06	290.2 ± 27.3	102.5 ± 8.2	114.8 ± 1.7
UC2	67.3 ± 3.2	1.8 ± 0.27	86.1 ± 0.4	2.2 ± 0.02	120.3 ± 9.1	76.4 ± 4.2	154.8 ± 1.7

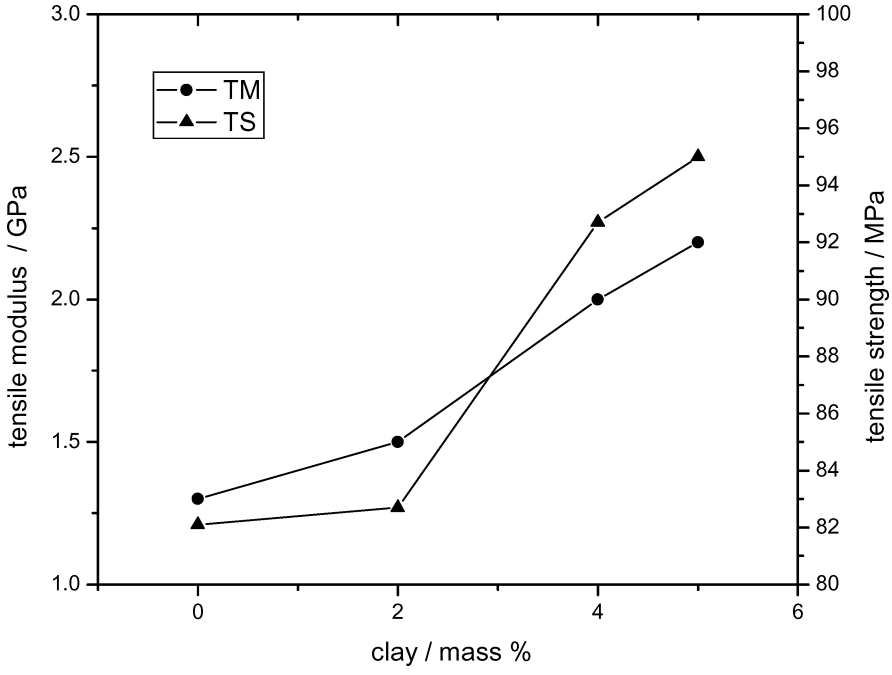

Fig. 6. Effect of clay loading on tensile strength and tensile modulus of PA6 (Y series).

3.2 SEM Observation

Figure 2 shows a schematic picture of the clay particle of several micrometers in size, which are aggregates of the clay plates. These are peeled off from the surface layer (which will form the exfoliated clay) and fragmented by the penetration of the polymer chain at the space between the clay plate aggregates where there is a difference in the direction of clay orientation. This picture also illustrates how the core residual particles are left untouched by the polymer chain due to the difficulty in accessing the core, as seen from the plasma-etched surface SEM. A direct observation of the surface morphology of the composite materials by scanning electron microscopy (SEM) is also shown in Figure 3 [a representative scanning electron micrograph of PA6 (Y series)]. It is clearly seen from this figure, that although exfoliated and intercalated silicate platelets are present at the nanoscale level there still exist micrometer-sized core residual particles (0.51 – 0.79 μm) in the composite.

3.3 Nanostructure and Morphology from XRD and TEM

Figure 4 (a,b,c) shows the WAXRD pattern for PA6, PA6/66 and its nanocomposites with different clay content. It is seen that the WAXRD pattern for PA6 shows two main reflections at about $2\theta = 21^\circ$ ($\alpha 1$) and 23.7° ($\alpha 2$) which belong to the monoclinic form ($\alpha 1$ arises from the distance between hydrogen bonded chains and $\alpha 2$- separation of hydrogen bond sheets). Therefore, it is evident that the α-form is the dominant crystalline phase for PA6. Besides these reflections, a further reflection is observed at around $2\theta = 10.7^\circ$ for the polyamide clay nanocomposites. This reflection is associated with the pseudo-hexagonal form (γ-form). From Figure 4a we see that as the clay loading percentage increases, there is a decrease in the intensity of the α-form and an increase in the intensity of the γ-form, thus indicating that an $\alpha \rightarrow \gamma$ crystal transformation occurs. The d-spacing due to the γ phase (0.82 nm) maintains its value over the whole range of clay loading. Also, the addition of clay induces the formation of the γ-form, which was seen in all cases (Fig. 4a, b, c), suggesting a heterogenous nucleation mechanism. In the higher clay percent nanocomposites such as Y4 and Y5, an additional diffraction peak occurs at around $2\theta = 4.7^\circ$ (d-spacing = 1.87 nm) and this probably indicates the formation of intercalated nanostructures. Figure 5a (i, ii, iii) and 5b (i, ii) shows the TEM micrographs of the polyamide clay nanocomposites. The morphology of the nanocomposites as seen from the TEM micrographs (Fig. 5a) clearly shows the dispersion of clay in the PA6 matrix. In the clay-loaded nanocomposites with mass fractions of clay 4% and 5%, intercalated clay aggregates are observed, in addition to the well-dispersed clay plates in the polymer matrix. Similar effects are seen in PA6/66 clay nanocomposites (Fig 5b (ii)). In Figure 5a, for more complete analysis of the structure of the organoclay in these polymer matrices, quantitative analyses of dispersed or stacked platelets in TEM photomicrographs (low magnification) were conducted. Image analysis data, given in Table 3, provide a quantitative comparison between the different clay contents. The particle population, which is the average number of particles per area (expressed as particles/μm^2), is a measure of the extent of exfoliation,

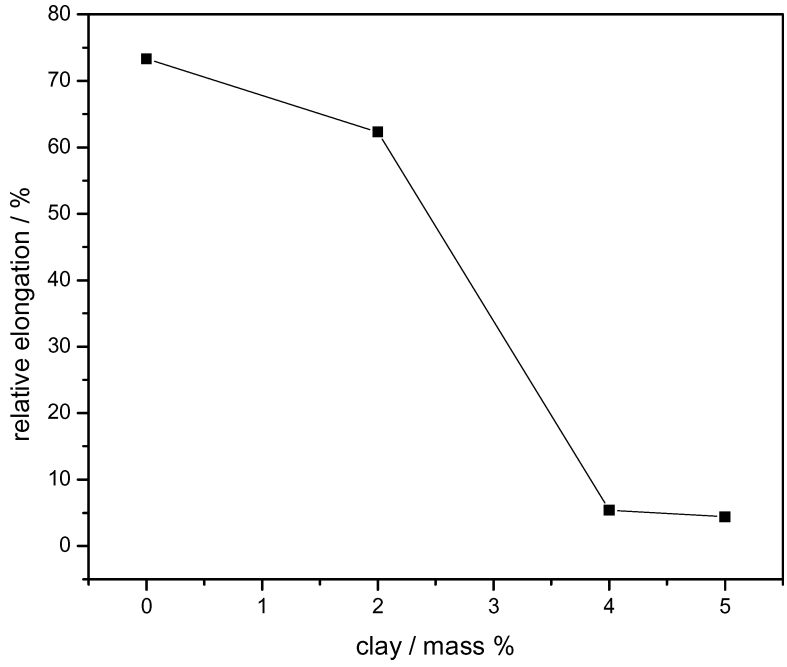

Fig. 7. Effect of clay loading vs Elongation of PA6 (Y series).

along with the average thickness of platelets and the standard deviation of thickness. As seen in Table 3, Y4 and Y5 showed higher values than Y2 in particle population. But the number of particles in Y4 is less than twice the number of particles in Y2, which implies that the residual core particle population is smaller in Y2. The average thickness of Y2 was 2.95 nm, which is smaller than Y4 or Y5, and which implies better dispersion of clay platelets in Y2. The coexistence of the exfoliated and intercalated nanoparticles as well as the micrometre-sized residual core particles in the SEM and TEM analyses provide a basis for the peeling and fragmenting process shown in Figure 2 during the clay incorporation step. Figure 5b (i) show a great degree of exfoliation structure.

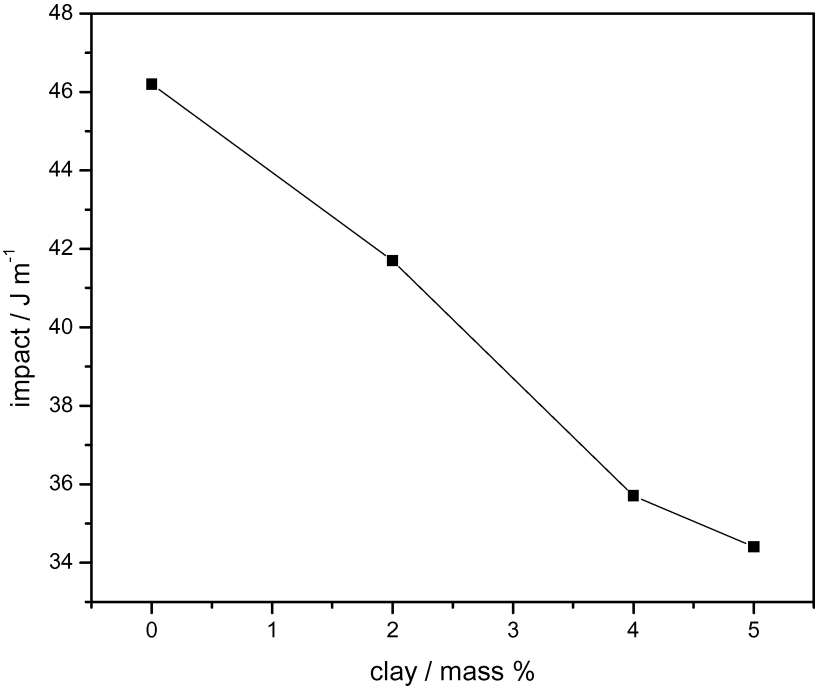

Fig. 8. Effect of clay loading on Impact strength of PA6 (Y series).

3.4 Mechanical Properties

The mechanical properties are summarized in Table 4. Plots of the effect of clay loading versus tensile strength & tensile modulus and elongation for the Y series are shown in Figures 6 and 7, respectively. The tensile strength and modulus both show a modest increase at 2% clay loading, but then show significant enhancement at 4% and 5% clay loading. The presence of the exfoliated single clay platelet in Y2 (Fig. 5a (i)) may not contribute to enhancement of the strength and modulus of the rigid Nylon matrix (T_g = 54°C), but the formation of bundles of several platelets in Y4 [Fig. 5a (ii)] and Y5 [Fig. 5a (iii)] may provide sufficient rigidity to the rigid matrix. Nylon-6/clay nanocomposites with 5% clay (Y5) showed a 69 % increase in tensile modulus and a 75% increase in flexural modulus. The increase in tensile strength and flexural strength with 5% clay loading was 16% and 27%, respectively. The relatively rigid bundle formation in Y4 and Y5 clearly dropped the elongation at break from 73% (Y0) to 4.4 % (Y5) (Fig. 7). The heat distortion temperature was raised by about 20°C with the presence of the clay (Table 4), but it decreased the impact strength (Fig. 8) of polyamide-6 although the effect of clay dispersity on impact strength is not clear and requires further micro-mechanical studies.

4 Conclusions

The thermal characteristics and morphology of the polyamide-6 & 6/66/clay nanocomposites, as well as the phase transformation between the α-form and the γ-form due to the introduction of clay loading into polymer matrix were studied. WAXRD and DSC data show that the loading of silicates has a heterophase nucleation effect which is favorable for the formation of γ-form crystals of PA6. Plasma-etched surface SEM and TEM studies indicate the coexistence of exfoliated, intercalated and residual core particles in the composite. As clay content in both polyamide-6 and polyamide6/66 increases, the thermal decomposition temperature (T_d) shows an increasing trend and hence an improvement in the thermal stability of the polymer. The addition of clay significantly leads to substantial improvement in the tensile properties.

Acknowledgement

The authors would like to thank UBE and UNITIKA Industries Ltd for providing the samples. The authors wish to thank Dr. S. Maeda for the molecular weight data measured by GPC. This work is a part of the IUPAC project (project #2003–051-400). One of the authors (Sriram.V.) wishes to thank the Ministry of Education for a BK21 post-doctoral fellowship.

References

1. Honma, I., Nomura, S. and Nakajima, H. (2001) *J. Membrane Sci.,* 185, 83–94.
2. Kawasumi, M. (2004) *J. Polym. Sci: Part A: Poly Chem.,* 42, 819–824.
3. Kojima, Y., Usuki, A., Kawasumi, M., Okada, A., Kurauchi, T., Kamigaito, O. and Kaji, K. (1994) *J. Polym. Sci. Polym. Phys*., 32:625–630.
4. Kojima, Y., Usuki, A., Kawasumi, M., Okada, A., Kurauchi, T., Kamigaito, O. and Kaji, K. (1995) J. *Polym. Sci. Polym. Phys*., 33:1039–1045.
5. Xie, S., Zhang, S., Zhao, B., Qin, H., Wang, F. and Yang, M. (2005) *Polym. Intl.,* 54, 1673–1680.
6. Fornes, T.D., Yoon, P.J., Keskkula H. and Paul, D.R. (2001) *Polymer,* 42, 9929–9940.
7. Fornes, T.D., Yoon, P.J., Hunter, D.L., Keskkula, H. and Paul, D.R. (2002) *Polymer,* 43, 5915–5933.
8. Liu, T.X., Tjiu, W.C., He, C.B., Na, S.S. and Chung, T.S. (2004) *Polym. Intl.,* 53, 392–399.
9. Liu, T.X., Liu, Z.H., Ma, K.X., Shen, L., Zeng, K.Y. and He, C.B. (2003) *Comp. Sci. & Tech.,* 63, 331–337.
10. Park, M.G., Sriram, V. and Kim, S.C. (2006) *J. Appl. Polym. Sci*., 101, 1711–1722.
11. Lincoln, D.M., Vaia, R.A., Wang, Z.G., Hsiao, B.S. and Krishnamoorti, R. (2001) *Polymer,* 42, 9975–9985.
12. Liu, X. and Wu, Q. (2002) Eur. *Polym. J.,* 38, 1383–1389.
13. Liu, X. and Wu, Q. (2002) *Polymer,* 43, 1933–1936.
14. Dabrowski, F., Bouribigot, S., Delobel, R. and Lebras, M. (2000) *Eur. Polym. J.,* 36, 273–284.
15. Krishnamoorti, R. and Yurskli, K. (2001) *Curr. Opinion Colloid Interface Sci*., 6, 464–470.
16. Russo, G.M., Nicolais, V., Di Maio, L., Montesano, S. and Incarnato, L. (2007) *Polymer Degradation and Stability*, 92, 1925–1933.
17. Shanmuganathan, K., Deodhar, S., Dembsey, N.A., Fan, Q. and Patra, P.K. (2008) *Polymer Engineering & Science,* 48, 662–675
18. Komarneni, S. (1992) *J. Mater. Chem.,* 2, 1219–1230.
19. Hill, P.G., Foot, P.J.S. and Davis, R. (1996) *Synth. Met*., 76, 289–292.
20. Mark, J.E. (1996) *Poly. Eng. Sci*., 36, 2905–2920.
21. Lebaron, P.C., Wang, Z., Pinnavaia, T.J. (1995) *Appl. Clay. Sci.,* 15, 11–29.
22. Kojima, Y., Matsuoka, T., Takashashi, H. and Kurauchi, T. (1993) *J. Mater. Sci. Lett.,* 12(21), 1714–1715.
23. Alexandre, M. and Dubois, P. (2000) *Mater. Sci. Eng.,* 28, 1–63.
24. Zhang, Y., Yang, J.H., Ellis, T.S. and Shi, J. (2006) *J. Appl. Polym. Sci.,* 100, 4782–4794.
25. Mathias, L.J., Davis, R. D. and Jarrett, W.L. (1999) *Macromolecules,* 32, 7958–7960.
26. Wu, T.M. and Liao, C.S. (2000) *Macromol. Chem. Phys.,* 201, 2820–2825.
27. Jimenez, G., Ogata, N., Kawai, H. and Ogihara, T. (1997) *J. Appl. Polym. Sci.,* 64, 2211–2220.
28. Ogata, N., Kawakage, S. and Ogihara, T. (1997) *Polymer,* 38, 5115–5118.